NANO LETTERS

2004
Vol. 4, No. 10
1863−1867

Yield Strength Asymmetry in Metal Nanowires

Jiankuai Diao,* Ken Gall, and Martin L. Dunn

Department of Mechanical Engineering, University of Colorado, Boulder, Colorado 80309

Received June 28, 2004; Revised Manuscript Received August 9, 2004

ABSTRACT

We performed atomistic simulations to study the yield mechanisms in gold nanowires. Perfect fcc gold nanowires all yield via the nucleation and propagation of {111}⟨112⟩ partial dislocations. The magnitude of the yield stress is much larger in tension versus compression for very small ⟨100⟩ nanowires, and this asymmetry is primarily due to the effects of surface stresses and different slip systems active during tensile and compressive yielding. Nanowires with a ⟨111⟩ orientation only show significant tension–compression asymmetry when defects exist in the wire prior to reverse compressive loading. The predictions may explain recent measurements regarding the yield of gold nanowires (see Marszalek, P. E.; Greenleaf, W. J.; Li, H. B.; Oberhauser, A. F.; Fernandez, J. M. *PNAS* 2000, *97*, 6282).

Metal nanowires are of great technological importance due to their potential applications in miniaturized electrical, optical, thermal, and mechanical systems. Nanowires have a large surface area/volume ratio as compared to bulk materials, and their structure and properties can be quite different than those of bulk materials. The use of nanowires in emerging technologies demands a thorough understanding of their structure and properties. Recent advances in the development of the experimental tools have made it possible to evaluate the mechanical properties of materials not only at nanometer scales, but also when the material samples have nanometer dimensions. For example, Marszalek et al.[1] impressively measured quantized plastic deformation in gold nanowires under tension and compression caused by individual slip events using atomic force microscopy. They also identified an asymmetry in the tension−compression yielding of gold nanowires, i.e., the magnitude of the tensile yield stress is much larger than that of the compressive yield stress in small nanowires. However, they did not provide a mechanistic explanation for this difference.

Atomistic simulations have been used by a number of researchers to study the inelastic deformation mechanisms in nanometer-scale materials subjected to various loading conditons.[2−13] However, these prior studies have not examined tension−compression asymmetry or aimed to understand the effect of surface stress on yielding. The objective in this work is to use atomistic simulations to investigate the effect of surface stress on the yielding of metal nanowires and explain the experimentally observed tension−compression yield stress asymmetry in gold nanowires.

We perform atomistic simulations with an embedded atom method (EAM) potential for fcc gold.[14] Gold nanowires oriented in the ⟨100⟩ direction with a square cross-section and (010) and (001) side surfaces were created with initial atomic positions corresponding to the bulk fcc lattice. We also performed simulations on ⟨$1\bar{1}1$⟩ nanowires with a nearly square cross-section and with ($\bar{1}\bar{1}2$) and ($1\bar{1}0$) side surfaces. Because of the tensile surface stresses in the side surfaces, the nanowires created with this initial structure are not in equilibrium and contract upon dynamic relaxation at 10 K. The equilibrium state is determined by allowing the contraction to saturate as a function of relaxation time. Periodic boundary conditions are used in the length direction, and we found that the equilibrium strain (with respect to the unrelaxed configuration) does not depend on the ratio of the periodic length to wire width in the dynamic relaxation.

Starting from the equilibrium configuration of the nanowires, we next performed uniaxial tensile and compressive loading on the relaxed nanowires until they yielded. We displaced all the atoms in accordance with a prescribed uniform strain in the length direction, fixed the periodic length in the length direction, and then dynamically relaxed the nanowires at 2 K for 200 ps with 0.004 ps per time step to obtain the equilibrium configurations of the nanowires at the prescribed strain. The equilibrium state of the nanowires was determined by allowing the stress to saturate as a function of time. The nanowires typically reach equilibrium after 100 ps and the stress averaged over the second 100 ps is used as the stress of the nanowires hereafter. We use the virial stress (Π^{ij}) for a system of atoms and the corresponding atomic level stress (π^{ij}) for individual atoms.[15−17] Due to the nature of uniaxial loading, only the stress component Π^{11} is nonzero and is simply denoted as Π; however, other components of π^{ij} can be nonzero for individual atoms. For each nanowire, we repeated the loading process until yield

* Corresponding author. Email: diao@colorado.edu.

10.1021/nl0489992 CCC: $27.50
Published on Web 08/26/2004

with a varying strain increment at each loading step. The yield stress does not depend on periodic length for a periodic length ranging from the wire width to eight times the wire width. Smaller periodic lengths may affect the yield stress, since dislocations may interact with images in the adjacent periodical cells.

To expedite simulations, we explored the possibility of using static simulation as an alternative in the first few steps well before yielding. We compared the exclusive dynamic uniaxial tensile loading with a combined static/dynamic uniaxial tensile loading of the 2.65 nm × 2.65 nm nanowire. In the combined uniaxial tensile loading, the nanowire is loaded statically in the first five steps and dynamically in the remaining steps. The two methods show little difference in both yield stress and yield strain, so this combined approach was used for all simulations.

In the simulations hereafter, the periodic length is fixed at three times the width, and the nanowires are loaded statically for the first few steps, followed by dynamic loading. During dynamic loading, the reported stress is the average stress over the second 100 ps. A large strain increment is used in the first several steps, then the step size is gradually reduced; the step size is reduced to 0.1% a few steps before yielding, and the step size is further reduced to 0.05% just before yielding.

The tensile surface stresses on the side surfaces cause the ⟨100⟩ and ⟨111⟩ wires to contract upon relaxation to equilibrium from the bulk lattice positions, with the magnitude of contraction increasing with decreasing cross-sectional area. At equilibrium, the tensile surface stress is balanced by induced compressive stress in the interior of the nanowires. When the cross-sectional area of an fcc ⟨100⟩ nanowire is larger than or equal to 2.45 nm × 2.45 nm, the contraction is elastic and less than 6%; however, when the cross-sectional area of an fcc ⟨100⟩ nanowire is less than 2.45 nm × 2.45 nm, yielding occurs upon relaxation via the nucleation and propagation of {111}⟨112⟩ partial dislocations.[18] We performed uniaxial loading on nanowires that do not yield upon relaxation.

Figure 1a shows representative stress (Π)−strain curves for ⟨111⟩ and ⟨100⟩ nanowires with a cross-section of about 4 nm × 4 nm under uniaxial tension and compression. The wires deform elastically until a critical point is reached and the wire yields. The initial yield results in a significant drop in stress in all cases under the displacement controlled loading. The strain in Figure 1a is measured with respect to the relaxed configurations.

Figure 1b shows the uniaxial tensile and compressive yield stress (Π_y) of the ⟨100⟩ nanowires as a function of the wire size and the ⟨111⟩ wire at one size. The magnitude of the tensile yield stress of the ⟨100⟩ wires increases slightly with a decrease of the wire cross-sectional area, while the magnitude of the compressive yield stress decreases. The magnitude of the tensile yield stress is significantly larger than that of the compressive yield stress for the ⟨100⟩ nanowires.

Yielding of the ⟨100⟩ nanowires occurs through the nucleation and propagation of {111}⟨112⟩ partial dislocations

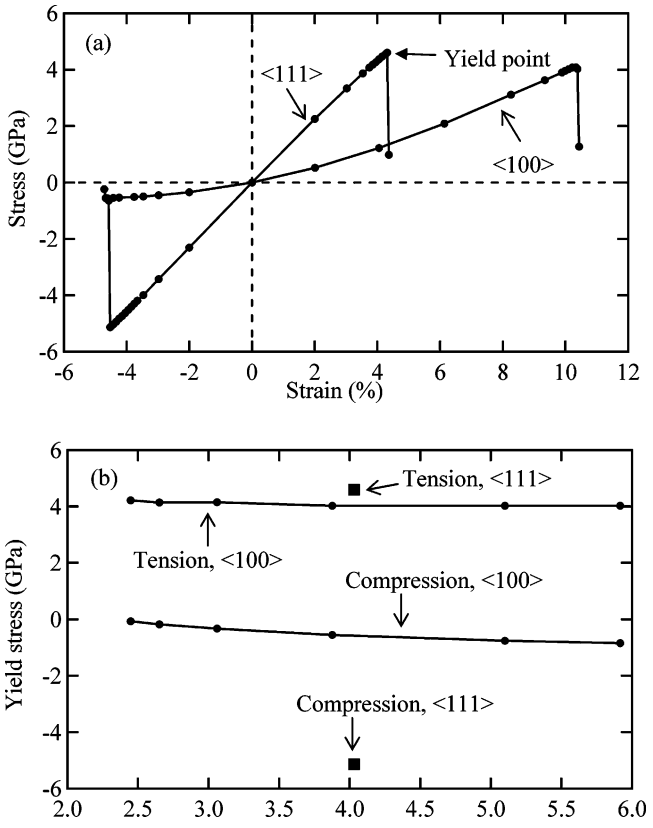

Figure 1. (a) Uniaxial tensile and compressive stress (Π)−strain curves for the fcc ⟨111⟩ and ⟨100⟩ nanowires with equivalent sizes near 4 nm × 4 nm and (b) the uniaxial tensile and compressive yield stress (Π_y) of the ⟨100⟩ nanowires as a function wire size and the ⟨111⟩ wire at one size.

(Figure 2). Partial dislocations nucleate from edges of the nanowires and propagate across the nanowires. Only the {111}⟨112⟩ partial slip occurs in compressive yielding, while in tensile yielding, both {111}⟨112⟩ partial and {111}⟨110⟩ perfect slips occur. The {111}⟨110⟩ perfect slip occurs through two {111}⟨112⟩ partial slips on the same {111} planes. The passage of the trailing dislocation under tensile loading, and not under compressive loading, is consistent with the higher uniaxial Schmidt factor of the trailing dislocation vs leading dislocation under tension, but not under compression for the ⟨100⟩ nanowires (Table 1). The slip mechanisms in ⟨111⟩ nanowires are the same as in ⟨100⟩ nanowires, i.e., the nanowires slip via {111}⟨112⟩ partial dislocation nucleation and propagation. In tensile yielding of the ⟨111⟩ nanowires, only partial {111}⟨112⟩ slip occurs, as in the case of compressive yielding of ⟨100⟩ nanowires. In compressive yielding of the ⟨111⟩ nanowires, both {111}⟨112⟩ and {111}⟨110⟩ slips occur and the {111}⟨110⟩ slip occurs through two successive {111}⟨112⟩ slips on the same {111} planes. As in the tensile yielding of the ⟨100⟩ nanowires, the passage of the trailing dislocation in the compressive yielding in the ⟨111⟩ nanowires is due to the larger uniaxial Schmidt factor in the trailing slip direction (Table 1).

Figure 3a shows the effective critical resolved shear stress (RSS) caused by the external forces in the leading slip

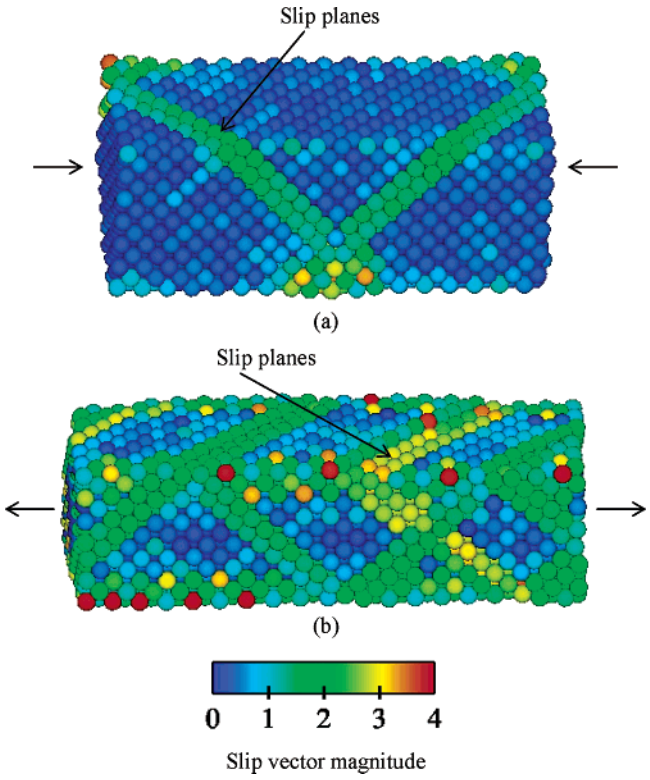

Figure 2. Active slip systems in the 2.65 nm × 2.65 nm fcc ⟨100⟩ nanowire in (a) tensile and (b) compressive yielding. Atoms are colored according to the slip vector magnitude.[24] The slip vector magnitude is 1.67 Å for a {111} ⟨112⟩ partial slip and 2.89 Å for a perfect {111}⟨110⟩ slip in gold. Consequently, blue atoms are in perfect fcc lattice, green atoms represent stacking fault (due to partial slip), and yellow atoms represent perfectly slipped atoms.

Table 1. Uniaxial Schmidt Factors, *m*, for the Most Favorable {111}⟨112⟩ Partial Slip Systems in ⟨100⟩ and ⟨111⟩ Nanowires under Uniaxial Tension and Compression

	compression		tension	
orientation	leading	trailing	leading	trailing
⟨100⟩	0.47 (4 systems)	0.24	0.24 (8 systems)	0.47
⟨111⟩	0.16 (6 systems, 0.79 Å[a])	0.31	0.31 (3 systems, 1.57 Å[a])	0.16

[a] Projection of the slip vector onto the uniaxial loading direction.

direction on the slip plane as a function of the wire size. The effective critical RSS is calculated by multiplying the uniaxial yield stress (Π_y) (Figure 1b) by the uniaxial Schmidt factor (m) (Table 1): $T_y = m\Pi_y$. Due to the large yield strain, we have taken into account the change to the uniaxial Schmidt factor caused by this large deformation in the calculation of the critical RSS by using the slip plane normal and slip direction just before yielding. Since the effective critical RSS depends on wire size, wire orientation, and loading conditions (tension vs compression), it cannot be used as a criterion or an indicator for the nucleation and propagation of a partial dislocation in nanowires; this motivates us to explore the detailed distribution of the RSS on the slip planes at the onset of yielding.

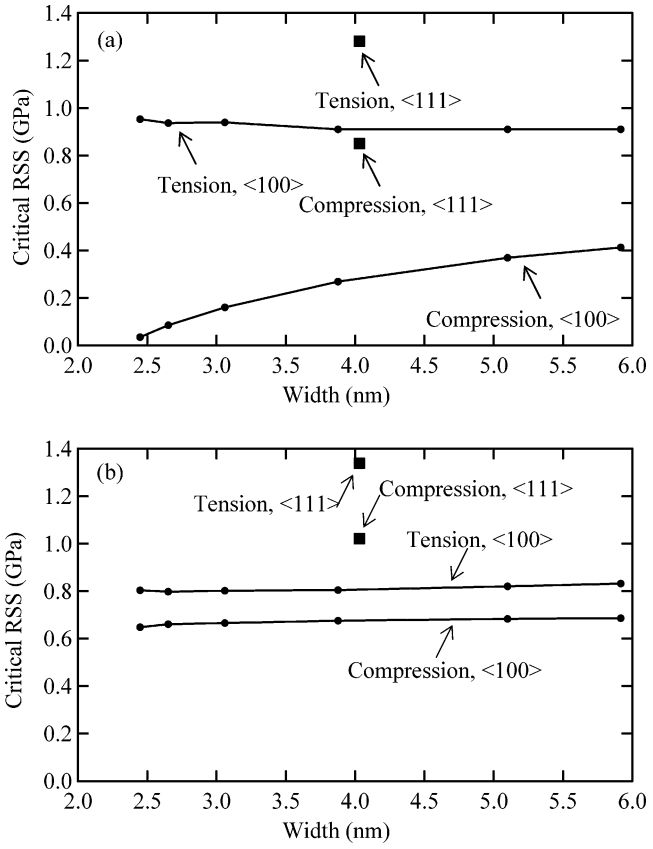

Figure 3. (a) Effective critical RSS (T_y) in the leading slip direction on the slip plane caused by the external forces and (b) the critical RSS ($\hat{\tau}_y$) averaged over the interior, which is caused by both the external forces and surface stresses, as a function of the ⟨100⟩ wire width, along with those of a ⟨111⟩ nanowire.

Figure 4 shows the RSS distribution in the slip direction on the {111} slip planes of the 2.65 nm × 2.65 nm ⟨100⟩ nanowire after relaxation and during the yield process. The RSS distribution is calculated by $\tau = \pi^{ij}\alpha^{ij}$, where $\alpha^{ij} = (1/2)(n^i t^j + n^j t^i)$ is the Schmidt factor tensor with n^i being the unit slip plane normal and t^j being the unit slip direction. Due to the large strain, we have again taken into account the change to the Schmidt factor tensor caused by this large deformation in the calculation by using the actual slip plane normal and slip direction. The RSS in the interior is essentially zero in the unrelaxed nanowires. For compressive yielding, the RSS has an average value of $\hat{\tau}_0 = 0.56$ GPa in the interior of the relaxed nanowire (Figure 4 a), and it increases to $\hat{\tau}_y = 0.66$ GPa at the onset of the compressive yielding (Figure 4b). The interior of a nanowire is defined to be all atoms excluding the outermost two layers. For tensile yielding, the RSS in the interior has an average value of $\hat{\tau}_0 = -0.28$GPa in the relaxed nanowire (Figure 4d), and it increases to $\hat{\tau}_y = 0.80$ GPa at the onset of tensile yielding (Figure 4e). The yielding of a nanowire consists of the nucleation and propagation of partial dislocations throughout the nanowire cross section. While the dislocation nucleation criterion in a general material is still a topic of considerable study,[19,20] dislocation nucleation in a nanowire seems related to the RSS in the interior. The nucleation event involves the dislocation moving away from its image at the surface,

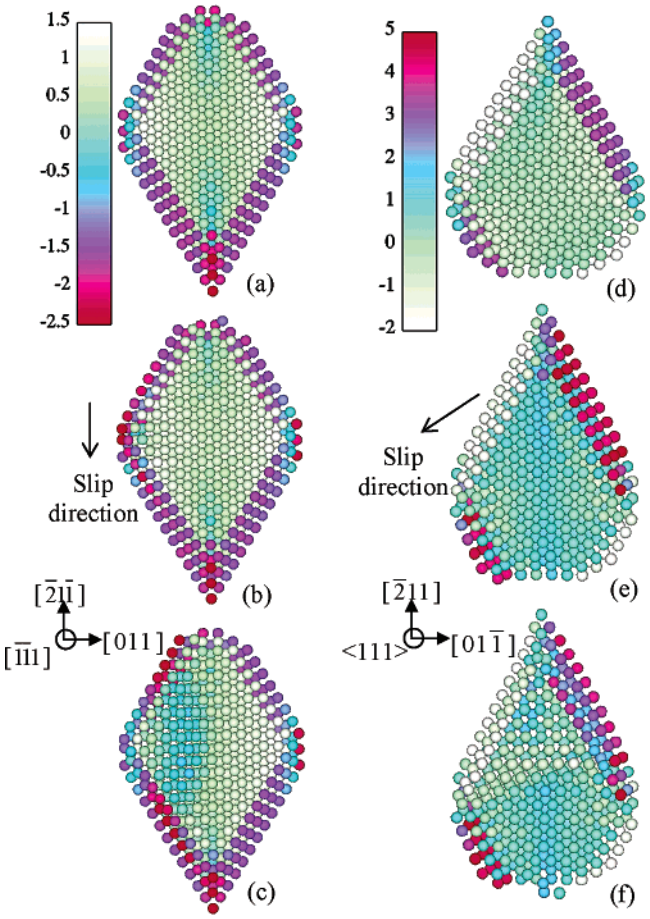

Figure 4. RSS distribution in the slip direction on the {111} slip planes of the 2.65 nm × 2.65 nm ⟨100⟩ nanowire after relaxation (a, d) and during the compressive (b,c) and tensile (e,f) yielding process. The positions of the slip planes in the nanowires are indicated in Figure 2. When the slip planes meet a periodic boundary, the slip continues on the opposite boundary, so only parts of the slip planes are shown here.

creating a stacking fault, which implies that there is a nucleation barrier at a critical distance from the surface. It is at this distance that the nanowire must attain a critical stress. An ill-defined dislocation may easily nucleate at a surface; a full-fledged dislocation nucleates only after the stress at a distance from the surface reaches a critical value. Since the RSS in the interior of the nanowire are quite uniform, its averaged value over the interior is calculated. Once nucleated, a dislocation will propagate throughout the nanowire since it is much easier to propagate a dislocation. Figure 4c and f shows the propagation of the partial dislocations in compressive and tensile yielding.

The critical RSS, $\hat{\tau}_y$, averaged over the interior of the ⟨100⟩ and ⟨111⟩ nanowires as a function of nanowire size, is shown in Figure 3b; it is caused by both the external forces and the surface stresses. The contribution from surface stress (Table 2) is through the its induced compressive stress in the interior of the nanowires. The critical RSS, $\hat{\tau}_y$, averaged over the interior of the ⟨100⟩ nanowires at the onset of compressive or tensile yielding does not change significantly with the nanowire size. Thus a more appropriate nanowire yielding criterion is that when the RSS, $\hat{\tau}$, averaged over the interior

Table 2. Surface Stresses (J/m^{-2}) in Gold Surfaces from the EAM (see ref 23 for the method of calculation) and Density Functional Theory (DFT)[21,22]

surface (i)	directions (j)	f_{ij}(EAM)	f_{ij} (DFT)
{100}	isotropic	1.57	4.57
{111}	isotropic	1.76	2.77
{1$\bar{1}$0}	⟨111⟩	1.32	
	<$\bar{1}\bar{1}$2>	1.11	
	shear	−0.31	
{$\bar{1}\bar{1}$2}	⟨111⟩	1.12	
	<1$\bar{1}$0>	1.37	
	shear	0	

of an ⟨100⟩ nanowire under compression or tension reaches a critical value, the nanowire yields. However, although this criterion accounts for wire size effects, it does not capture the orientation or loading condition dependence of yield.

The difference between $\hat{\tau}_y$ and T_y is the contribution from the surface stresses ($\hat{\tau}_y - T_y$). By comparing $\hat{\tau}_y$ (Figure 3b) and T_y (Figure 3a), we see that the smaller the nanowire, the larger the contribution from surface stress in compressive yielding and, when the nanowire cross-sectional area is less than 2.45 nm × 2.45 nm, the nanowire yields under its own surface stress and no external force is necessary. For tensile yielding, the magnitude of T_y is larger than $\hat{\tau}_y$, which means that the contribution from the surface stresses ($\hat{\tau}_y - T_y$) and that from the external forces (T_y) have opposite signs and the external forces must overcome the RSS induced by the surface stress. Smaller nanowires have a larger RSS magnitude caused by the surface stress that the external forces have to overcome. Also, the uniaxial Schmidt factor (Table 1) for leading partial slip is larger under compression than under tension for ⟨100⟩ nanowires, and thus it is easier for ⟨100⟩ nanowires to yield under compression. Thus the asymmetry in the tension-compression yield in ⟨100⟩ nanowires is mainly caused by the biased surface stresses and different slip systems active during tensile and compressive yielding.

For the ⟨111⟩ nanowires, a shear surface stress component also exists on its (1$\bar{1}$0) surfaces (Table 2), in addition to the normal surface stress components. This shear surface stress causes a shear stress in the interior of the ⟨111⟩ nanwire upon relaxation. Note that the leading partial Schmidt factor is larger under tension versus compression for the ⟨111⟩ nanowires, but the surface stress contributes to the compressive yielding. These two opposing factors tend to balance each other and make the yield stress of the ⟨111⟩ nanowire quite symmetric, in contrast to the ⟨100⟩ nanowires (Figure 1a). The critical RRS, $\hat{\tau}_y$, values averaged over the interior of the ⟨111⟩ nanowire just before compressive and tensile yielding are also shown in Figure 3b. The critical RSS, $\hat{\tau}_y$, averaged over the interior of the nanowires, are different under tension and compression and for different orientations (Figure 3b), suggesting a lack of a universal Schmidt law based yielding criterion, even if the surface-stress-induced intrinsic stresses are taken into consideration.

At first observation, our results seemingly contradict the experimental observation by Marszalek et al.[1] in two

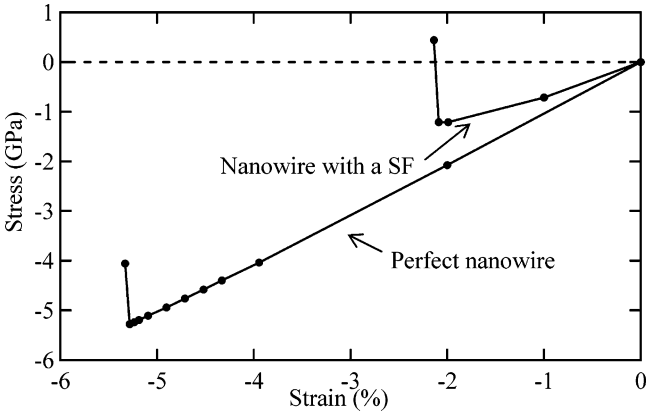

Figure 5. Compressive stress−strain curves of a perfect ⟨111⟩ nanowire (1.75 nm × 1.88 nm) and of the same nanowire with a preexisting stacking fault in it. The strains are calculated with respect to the relaxed configurations of the corresponding wires. The relaxed nanowire with a stacking fault is 1.47 Å longer than the relaxed perfect nanowire due to the slip that causes the stacking fault.

aspects: (i) we do not predict the large tensile-compressive strength asymmetry in ⟨111⟩ nanowires that they observed in experiments; (ii) they observed quantized displacement at multiples of 1.56 Å in both tensile and compressive inelastic deformation; however, the projection of the active slip vector in compressive loading onto the loading direction (0.79 Å) is only half of the observed value (Table 1) for a perfect ⟨111⟩ nanowire. These discrepancies can be explained by the preexistence of stacking faults in the ⟨111⟩ nanowires. Marszalek et al.[1] first pulled the nanowires in their experiments and presumably created stacking faults in the nanowires. Because the trailing Schmidt factor is smaller than the leading one under tension, it is more difficult to move trailing dislocations than to move new leading dislocations, thus the stacking faults have no driving force to dissolve under further tensile loading. When the same nanowire was compressed, they induced reverse slip, in the opposite direction of the original tensile slip on the same slip plane. This occurs because the uniaxial Schmidt factor for the reverse slip under compression, which is the same as that for tensile loading (0.31), is larger than the uniaxial Schmidt factor under compression for perfect ⟨111⟩ nanowires (0.16) (Table 1). This reverse slip explains the observed symmetric quantized displacement in the tensile and compressive yielding. Also, since the uniaxial Schmidt factors for the tensile loading and the reversed slip movement are the same, and the surface stress contributes to the RSS under compressive loading, the surface stress effect causes tensile and compressive strength asymmetry, which they experimentally observed in ⟨111⟩ nanowires.

To verify the above postulate, we performed tensile and compressive loading on ⟨111⟩ nanowires of approximately the same size (1.75 nm × 1.88 nm) as in experiments.[1] After the relaxation of the nanowire, we separately pulled and the compressed the nanowire and obtained a tensile yield stress of 4.9 GPa and a compressive yield stress of −5.3 GPa, which is quite symmetric. We then relaxed the ⟨111⟩ nanowire that yielded under tension without applying any force on it. The nanowire contracted to equilibrium and the stacking fault remained. We then compressed it; the wire underwent reverse slip and we obtained a yield stress of −1.2 GPa (Figure 5), the magnitude of which is much smaller than that of the compressive yield stress of a perfect nanowire (−5.3 GPa). We note that the surface stress of the EAM potential used is smaller (Table 2) than that from density functional theory calculations,[21,22] which implies that we may underestimate the surface stress effect. This may explain why the asymmetry in our simulations is smaller than observed in experiments.

In summary, we have shown that there are several key factors to consider in the yielding of metal nanowires: (1) intrinsic stress in the wire caused by surface stress, (2) active slip systems for nucleation and propagation of dislocations, (3) possible preexistence or complete absence of defects such as stacking faults or dislocations, and (4) surface and corner controlled defect nucleation. The aforementioned issues lead to a notably different yield behavior in nanowires relative to bulk single crystal and polycrystalline materials.

Acknowledgment. We thank the anonymous reviewer for his/her insightful comments on the manuscript. We also thank Dr. Steve Plimpton from Sandia lab for letting us use his ParaDyn code.

References

(1) Marszalek, P. E.; Greenleaf, W. J.; Li, H. B.; Oberhauser, A. F.; Fernandez, J. M. *PNAS* **2000**, *97*, 6282.
(2) Horstemeyer, M. F.; Baskes, M. I.; Plimpton, S. J. *Acta Mater.* **2001**, *49*, 4363.
(3) Sorensen, M. R.; Randbyge, M.; Jacobsen, K. W. *Phys. Rev. B* **1998**, *57*, 283.
(4) Kang J. W.; Hwang, H. J. *Nanotechnology* **2001**, *12*, 295.
(5) Liang, H. Y.; Wang, X. X.; Wu, H, G.; Wang, Y. *Acta mecnanica sinica* **2002**, *34*, 208.
(6) Landman, U.; Luedtke, W. D.; Burnham, N. A.; and Colton, R. J. *Science* **1990**, *248*, 454.
(7) Ikeda, H.; Qi Y.; Cagin, T.; Samwer, K.; Johnson, W. L.; Goddard, W. A. *Phys. Rev. Lett.* **1999**, *82*, 2900.
(8) da Silva, E. Z.; da Silva, A. J. R.; Fazzio, A. *Comput. Mater. Sci.* **2004** *30*, 73.
(9) da Silva, E. Z.; Novaes, F. D.; da Silva, A. J. R.; Fazzio, A. *Phys. Rev. B* **2004**, *69* 15411.
(10) da Silva, E. Z.; da Silva, A. J. R.; Fazzio, A. *Phys. Rev. Lett.* **2001**, *87* 256102.
(11) Wu, H. A.; Soh, A. K.; Wang, X. X.; Sun, Z. H. *Key Eng. Mater.* **2004** *261−263*, 33.
(12) Mehrez, M.; Ciraci, S.; Fong, C. Y.; Erkoc, S. *J. Phys.: Condens. Matter* **1997**, *9*, 10843.
(13) Finbow, G. M.; Lynden-Bell, R. M.; McDonald, I. R. *Mol. Phys.* **1997** *92*, 705.
(14) Foiles, S. M.; Daw, M. S.; Baskes, M. I. *Phys. Rev. B* **1986**, *33*, 7983.
(15) Egami, T.; Maeda, K.; Vitek, V. *Philosophical Magazine A* **1980** *41*, 883.
(16) Cheung, K. S.; Yip, S. *J. Appl. Phys.* **1991**, *70*, 5688.
(17) Zhou, M. *Proc. R. Soc. London A*, **2003**, *459*, 2347.
(18) Diao, J.; Gall, K.; Dunn, M. L. *Phys. Rev. B*, 2004a, in press.
(19) Miller, R. E.; Acharya, A. *JMPS* **2004**, *52*, 1507.
(20) Li, J.; Van Vliet, K. J.; Zhu, T.; Yip, S.; Suresh, S. *Nature* **2002**, *418*, 307.
(21) Needs, R. J.; Godfrey, M. J.; Mansfield, M. *Surf. Sci.* **1991**, *42*, 215.
(22) Fiorentini, V.; Methfessel, M.; Schoffler, M. *Phys. Rev. Lett.* **1993**, *71*, 1051.
(23) Diao, J.; Gall, K.; Dunn, M. L. *JMPS*, **2004b**, *52*, 1935.
(24) Zimmerman, J. A.; Kelchner, C. L.; Lein, P. A., Hamilton, J. C.; Foiles, S. M. *Phys. Rev. Lett* **2001**, *87*, 165507.

NL0489992